CORONA(E) OF AR LACERTAE. II. THE SPATIAL STRUCTURE

M. SIARKOWSKI

Space Research Center, Polish Academy of Sciences, Kopernika 11, 51-622 Wrocław, Poland; msiark@ii.uni.wroc.pl

P. PREŚ

Astronomical Institute, Wrocław University, Kopernika 11, 51-622 Wrocław, Poland; pres@astro.uni.wroc.pl

AND

S. A. DRAKE,[1] N. E. WHITE, AND K. P. SINGH[2]

Code 660.2, Laboratory for High Energy Astrophysics, NASA/GSFC, Greenbelt, MD 20771;
drake@lheavx.gsfc.nasa.gov, white@adhoc.gsfc.nasa.gov, singh@tifrvax.tifr.res.in

ABSTRACT

The X-ray light curves in the 0.4–1.5 keV and 2–7 keV bands of the RS CVn binary AR Lacertae observed on 1993 June 1–3 over one full orbital cycle with the *ASCA* satellite have been used to map the spatial structure of AR Lac's coronae. We find that both stars are X-ray active, that the corona of the K-type secondary star appears to be hotter than that of the G-type primary star, that X-ray emission is concentrated on the sides of the stars facing each other, and that there are compact and well-localized regions of enhanced X-ray emission with heights much smaller than the stellar radii. In one class of solutions there are additional extended regions with dimensions similar to or greater then the radii of the underlying stars which may be structures that interconnect the two stars. There are also other acceptable models without extended structures, however our analysis indicates that solutions with extended sources are more probable. Also, about 50% of the X-ray emission is unmodulated and could come from either an extended halo region, from the poles of the larger K star, or from other symmetric or uneclipsed structures in the orbital plane. We compare the coronal structures inferred from the *ASCA* observations with those inferred using the same technique from an *EXOSAT* observation of AR Lac made in 1984 and find that there are substantial differences between the coronal structures at these two epochs. For the solution with extended material in the orbital plane, we have derived the rough physical parameters for the X-ray–emitting plasma, using the derived information on the spatial sizes of the various spatial components together with information about the emission measure and temperatures obtained from a simple spectral analysis of the *ASCA* data.

Subject headings: binaries: eclipsing — stars: coronae — stars: individual (AR Lacertae) — X-rays: stars

1. INTRODUCTION

The RS CVn stars are among the most active late-type stellar coronal X-ray sources, having X-ray luminosities L_X that are 1000–30,000 times larger than the 10^{27} ergs s^{-1} value for the quiet Sun. They are close binary systems where the tidally enforced rapid rotation of the component stars is believed to interact with the convective motions in their outer envelopes so as to drive a powerful magnetic dynamo, resulting in high levels of chromospheric and coronal activity. The subset of eclipsing RS CVn systems has been the focus of much attention because the eclipse and orbital modulation can be used to map their coronal spatial distributions.

AR Lac is a relatively nearby (~ 50 pc) eclipsing RS CVn system and, due to this proximity and to its high $L_X \simeq 10^{31}$ ergs s^{-1}, is one of the brightest observable stellar coronal X-ray systems. It contains a 1.54 $R_\odot$ G2 IV primary with a 2.81 $R_\odot$ K0 IV secondary, separated by 9.22 $R_\odot$ (Chambliss 1976).[3] The orbital inclination is 87°; the primary eclipse is total, and the secondary eclipse is annular. The relatively short orbital period of 1.98 days is quite well suited to the

typical amounts of observing time available for individual targets with recent and current X-ray astronomy satellites, and, therefore, in the last two decades, several observations have been carried out to determine its X-ray orbital light curve.

The first extended X-ray observations of AR Lac were made using the *Einstein Observatory* in 1979–1980 (Swank & White 1980; Walter, Gibson, & Basri 1983). These early observations did not obtain complete coverage of an entire orbital cycle but, even so, did exhibit features in the light curve around the time of each eclipse that suggested localized emission regions on each star (Walter et al. 1983). There was evidence for X-ray eclipses at both minima in both the IPC (0.1–4 keV) and MPC (2–10 keV). Subsequent to this, *EXOSAT* observed AR Lac for a full orbital cycle in 1984, with almost continuous coverage (White et al. 1990). During the primary eclipse (when the G-type primary star is occulted by the K-type secondary star) the Low Energy (LE) experiment 0.05–2 keV light curve showed a 50% reduction in flux. The Medium Energy (ME) detector 1–6 keV light curve, in contrast, showed no strong modulation. The X-ray spectra of RS CVn stars measured with the *Einstein* SSS and *EXOSAT* Transmission Grating Spectrometer (TGS) show at least two temperature components to be present at 5–7 and 15–40 MK (Swank et al. 1981; Lemen et al. 1989). The deep modulation in the LE light curve suggests that compact lower temperature structures are present close to the surface of one or both of the component

---

stars. The ME light curve is dominated by the hotter component, and the lack of any strong modulation suggests this component comes from a large region comparable in size to the binary system dimensions. Similar results were obtained from *EXOSAT* observations of another eclipsing RS CVn system, TY Pyx (Culhane et al. 1990), and of the active binary system, Algol (White et al. 1986). In contrast to the *EXOSAT* results, observations of AR Lac in 1990 by the *ROSAT* PSPC in the 0.1–2.0 keV spectral band show $\simeq 50\%$ modulation centered on the primary eclipse but with no evidence for a reduction in the modulation amplitude at higher energies (Ottmann, Schmitt, & Kürster 1993). An *ASCA* observation of one orbital cycle of AR Lac made in 1993 shows a $\simeq 50\%$ minimum in the 0.4–7 keV band at primary eclipse and a similar amplitude at higher energies (White et al. 1994). These more recent results have cast some doubt on the original *EXOSAT* medium-energy result, which was obtained with a collimated proportional counter, unlike the *Einstein* IPC, *EXOSAT* low-energy, *ROSAT*, and *ASCA* observations which were made with imaging telescopes. Imaging telescopes generally provide a much higher signal to noise and more reliable determination of the background than collimators. It has been suggested (Schmitt 1994, private communication) that the *EXOSAT* ME result may have suffered from unreliable background subtraction, which masked out the modulation. The *ASCA* analysis of White et al. (1994) also shows that the ME light curve might be relatively more affected by flaring activity than the low-energy light curve, and they suggested that another possible explanation for the *EXOSAT* ME light curve is that a flare may have "filled in" the eclipse. These alternate suggestions could also explain the similar lack of an medium-energy modulation for TY Pyx (Culhane et al. 1990) and Algol (White et al. 1986)

Extensive modeling of the *EXOSAT* LE light curve of AR Lac was made by White et al. (1990) to determine the three-dimensional spatial structure. Both χ^2 fitting to idealized emission regions and a maximum entropy method (MEM) were employed. In both cases there were multiple solutions, which reduced to two patterns of compact emission regions on the two stars, and a large uneclipsed extended region. The peak electron pressure in the compact regions was found to be 100–200 dyne cm^{-3}, very similar to the values found in solar flares. In some model solutions a second more extended structure with a height of 10^{11} cm was required, with peak pressures 10–100 times lower. More recently Siarkowski (1992) used an iterative method for the three-dimensional deconvolution of the X-ray light curve to map the corona of AR Lac from the *EXOSAT* light curve. He finds that both stars have active coronae with many solar-like structures, with the largest having sizes greater than the stellar radii. This latter solution contains nearly all the possible discrete coronal structures found by White et al. (1990).

In this paper we have applied the same iterative technique as used by Siarkowski (1992) to analyze the X-ray light curves of AR Lac in two different energy bands that were obtained by *ASCA* in 1993, allowing us to make inferences about the spatial distribution of the corona(e) of AR Lac. In § 2, we give the details of the *ASCA* observation, while in § 3 we briefly describe the deconvolution technique that we have applied. In § 4, we present the results of this specific light-curve analysis, as well as an illustrative combined analysis in which we use the ratio of the two X-ray

light curves to derive information on the temperatures of the inferred spatial structures. In § 5, we compare these results both with a similar analysis that Siarkowski (1992) carried out on the *EXOSAT* light curve of AR Lac as well as with other light-curve studies that have used somewhat different techniques. In § 6, we discuss in some detail the various physical arguments for and against the existence of extended coronal features, and in § 7 we present our conclusions.

A companion paper (Singh, White, & Drake 1996) to the present one presents the results of a detailed analysis of the *ASCA* (and simultaneously obtained *ROSAT*) spectrum obtained during this AR Lac observation. In addition, an exhaustive discussion of the forms of the coronal emission measure distribution that are consistent with these X-ray spectra is presented by Kaastra et al. (1996).

2. OBSERVATIONS

AR Lac was observed by *ASCA* from 1993 June 1 to June 3. The observation covers slightly over one orbital period. The *ASCA* instruments consists of two pairs of spectrometers, solid state imaging spectrometers (SIS0 and SIS1) and gas imaging spectrometers (GIS2 and GIS3). A description of the instrumentation is given in Tanaka, Inoue, & Holt (1994). The details of the AR Lac observations are presented in White et al. (1994) and Singh et al. (1996). In the present paper, we construct a light curve in the 0.4–1.5 keV band by combining the data from the two SIS detectors, and one between 2–7 keV using the two GIS detectors. These energy bands were chosen so that the contributions from the low-temperature (~ 7 MK) component and the high-temperature (~ 23 MK) component, inferred from the detailed spectral analysis of the *ASCA* data by Singh et al. (1996), might be crudely isolated. This separation, however, works only in the 2–7 keV energy range which has little ($\simeq 5\%$) contribution from the low-temperature component. In the low-energy light curve, the contributions of the low-T and high-T components are 55% and 45%, respectively. The background-subtracted light curves are shown in Figure 1 folded on the ephemeris JD 2,444,114.3431 + 1.9831674E (Kim 1991). Both SIS and GIS light curves show significant reduction in counting rate at the times of both primary and secondary eclipses. During the primary eclipse (orbital phase 0.0) there is a reduction of $\sim 45\%$ in the SIS count rate and $\sim 55\%$ in the GIS count rate. The secondary eclipse at phase 0.5 is shallower and somewhat longer duration than the primary eclipse, with the corresponding maximum reduction in the count rates being $\sim 15\%$ and $\sim 25\%$ in the SIS and GIS detectors, respectively. A number of small flares are evident in both the GIS and the SIS data. These flares last from 20 to 60 minutes, and they are more pronounced in the GIS (2–7 keV) light curve, e.g., the particularly clear example of a flare visible at phase ~ 0.56. Also shown in Figure 1 is the hardness ratio (the ratio of the 2–7 keV/0.4–1.5 keV counts) to give an indication of the spectral variability. There is some evidence for a softening of the emission, e.g., before phase 0.2, during the secondary eclipse, and at phase 0.75, but overall there is not a strong modulation of the hardness ratio. These spectral changes are only significant at the 2.5 σ level, however; i.e., with 95% confidence we can state that the hardness ratio at these three phases differs from its "normal" value. Most of the observed short timescale fluctuations in the hardness ratio are connected with the flaring activity.
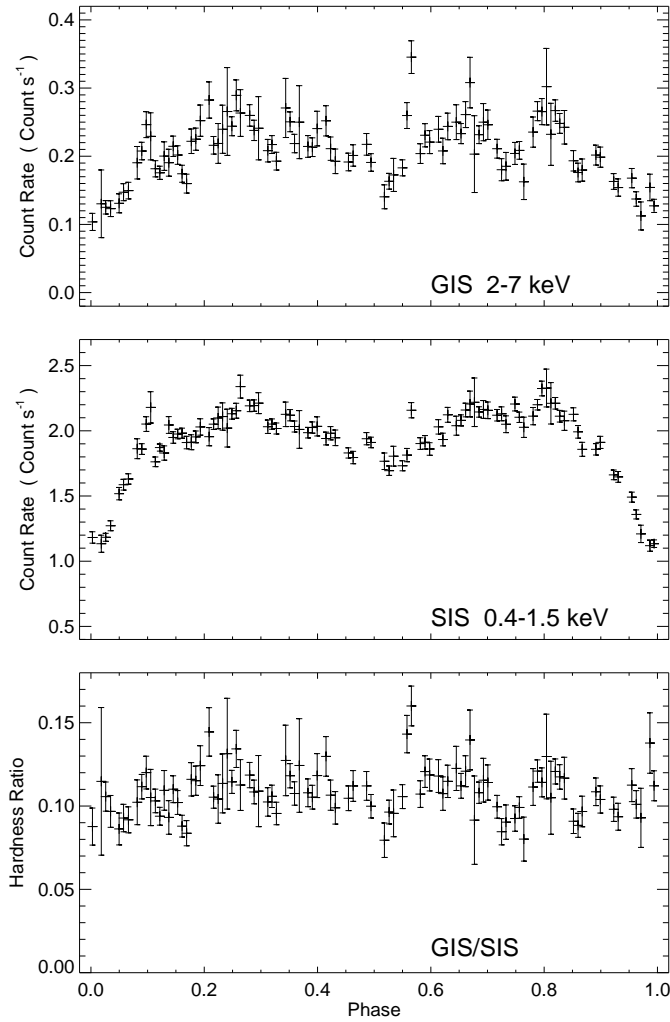
FIG. 1.—X-ray light curves of AR Lac in the GIS (*top*) and SIS (*middle*) detectors. Accumulation time is 1360 s. Errors correspond to 1 σ. The bottom panel shows the GIS/SIS count-rates ratio.

3. ITERATIVE DECONVOLUTION TECHNIQUE

A detailed mapping of the distribution of X-ray emitting material within the AR Lac system was made using the iterative deconvolution technique described by Siarkowski (1992). This method reconstructs the three-dimensional distribution of the X-ray emission from the observed light-curve modulation. The three assumptions involved in the application of this method are (1) X-ray emission is optically thin, (2) spatial structure of emission is stable over one orbital period, and (3) the binary system rotates as a rigid body. Usually we adopt such volume size that all the structures needed to explain the light curve are contained in the volume. To allow a direct comparison to be made between the *ASCA* results and those from the *EXOSAT* we selected the same volume as in the case of *EXOSAT*, viz., $23.1 \times 13.5 \times 2.7 \ R_\odot^3$. A grid size of $dx = dy = dz = 0.3 \ R_\odot$ was defined around the system. The spatial resolution is defined by the shift of the edge of each occultation strip for each step in phase. This shift strongly depends on localization of a given pixel in the considered volume. For nearly 100 points in one orbit the phase step is $3°6$. This is the change in the angle of the edges of occultation strips and gives a

linear shift of $l = r \sin (\Delta\phi)$, where r is the distance from the center of occulting star. The resolution, l, is 0.09 $R_\odot$ and 0.18 $R_\odot$ on the primary and secondary, respectively. At the center of mass $l \sim 0.3 \ R_\odot$ and at the edges of considered volume $l \sim 1 \ R_\odot$.

For simplicity an inclination of 90° was assumed (giving symmetry with respect to the orbital plane) so that in the vertical direction only one half-space need be considered, with z varying from 0 to 2.7 $R_\odot$. The iteration process was started assuming a uniform distribution of emission in the whole volume. This means that *the only assumption* made about the emitting structures was that they are localized inside the considered volume, but nothing was assumed about their number and size (except for the previously assumed grid size). The quality of the solution was measured in terms of the χ^2 between the calculated and observed light curves. The iterative process was stopped when the reduced value of $\chi^2 \sim 1.0$ was reached, since forcing a further reduction in the χ^2 can lead to modeling of the statistical errors leading to unrealistically sharp structures, as opposed to the modeling of the smooth components of the light curve. For the analysis of the quiescent corona we removed the most outstanding flarelike events at phases 0.09, 0.26, 0.56, 0.67, and 0.80. We have also tested our method for small perturbations of the binary system parameters and found it to be stable.

4. RESULTS OF THE ANALYSIS

In the first two subsections of this section we discuss the results that we obtain when analyzing the SIS and GIS light curves using initial models that have uniform emission distributions (excluding of course the volumes occupied by the stars themselves). The class of solutions that are thereby found tend, not surprisingly, to have significant emission that is fairly well distributed throughout the available volume, i.e., extended emission is not only "allowed" but somewhat preferred. In § 4.3, we additionally use the hardness ratio of the X-ray emission so as to infer the temperature and density of the various spatial regions. Finally, in § 4.4, we discuss the results that are obtained when we restrict the volume of space in which X-ray emission can occur to be close to the surfaces of the two stars.

4.1. *Modeling of the SIS* 0.4–1.5 keV *Light Curve*

The results of the deconvolution of the low-energy light curve are presented in Figure 2. The upper part of the figure shows the image of the corona as viewed by an observer located above the orbital plane. The middle part shows a side view of the system for a phase of 0.25 (an angle of 90°). At the bottom the observed and the calculated light curves are overlaid. In this figure we can distinguish a few well localized structures of emission, most of them located in between the stars. The largest and most prominent structure is anchored to the G primary (region a). This structure is elongated up to 2 solar radii and is further extended by the next center of emission (region b). Some small and less prominent structures are located near the surface of the secondary K giant (regions c, d, and g). The regions located near the surfaces of both stars could be considered to be analogs of solar X-ray active regions but scaled to much larger sizes. The highly located structures could either be the top of a large loop, or part of a magnetic structure interconnecting the two stars (see Uchida & Sakurai 1984). There is also a weak and diffuse structure located above the
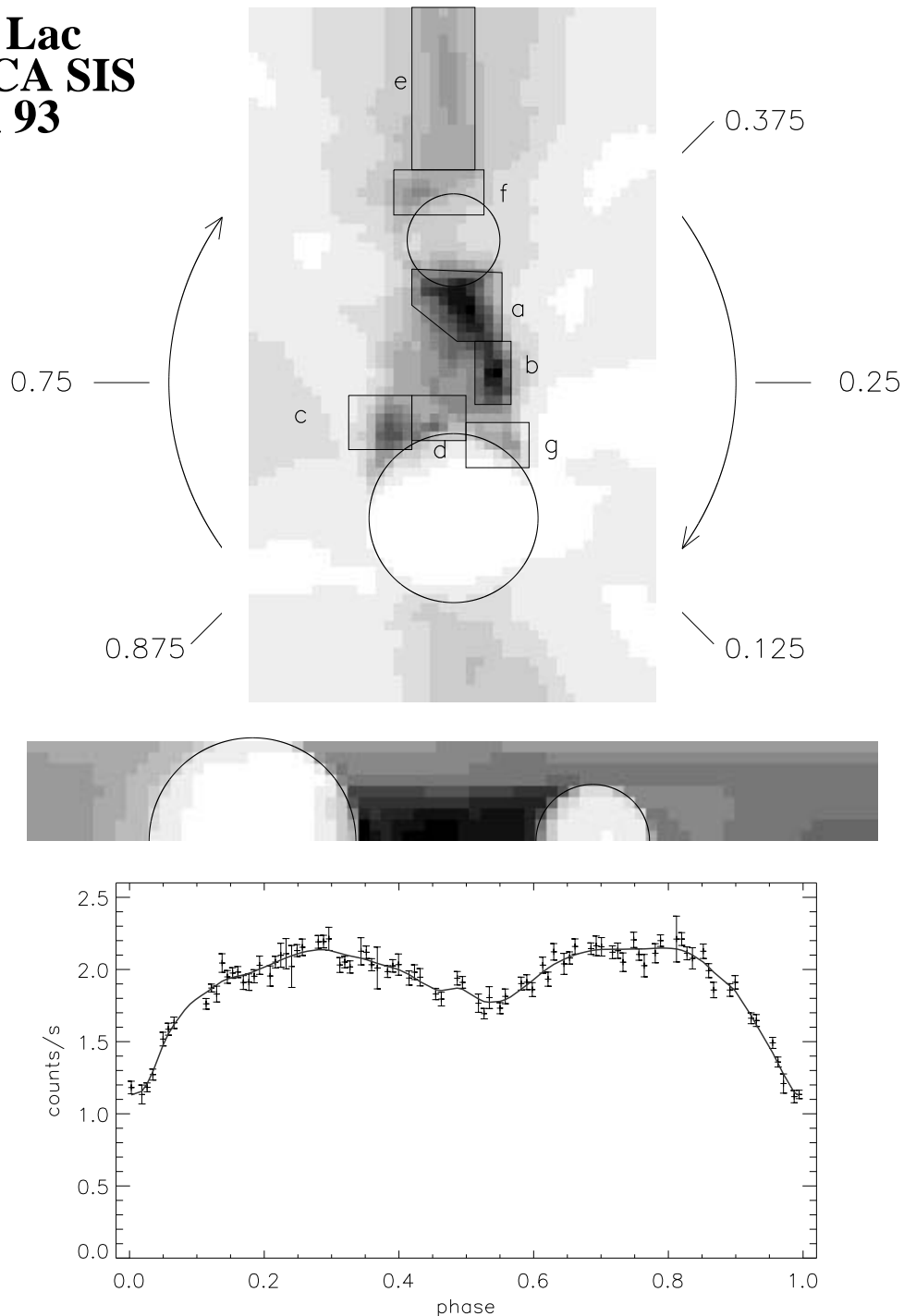
AR Lac
ASCA SIS
Jun 93

FIG. 2.—Results of the deconvolution of the SIS light curve with the flares removed as described in § 2, when obtained in 400 iteration steps. *Top*: image of the corona as viewed by an observer located above the orbital plane. *Middle*: side view of the system for a phase angle of 0.25 (90°). *Bottom*: observed and the calculated light curves are overlaid; the calculated light curve fits the observed one with a reduced $\chi^2 = 1.005$.

face of the primary facing away from the secondary star (region e). It extends on a scale of more than 6 $R_\odot$, i.e., to the edge of the volume modeled in this analysis. It bears some morphological resemblance to the streamer structures often observed in the white light and X-ray solar corona. Finally, beside this structure another weak region (denoted as f) can be distinguished near the surface of the G star. All prominent structures are located near the orbital plane. They are almost fully occulted during the time of the primary eclipse.

In the modeling a large percentage of the X-ray emission is not localized and must either be uniformly distributed throughout the volume or located at high latitudes on the larger K star. The evidence for this extended emission follows from the fact that there is a considerable ($\simeq 50\%$) residual emission during the primary eclipse, when most of resolved structures are occulted. This extended "halo" emission is particularly evident in the side view shown in Figure 2. Although its surface brightness is low, if we consider the volume occupied of this "halo" the total contribu-

tion constitutes ∼45% of the total emission. This "halo" emission could also come from structures that are symmetric or in an area outside the considered volume and thus have no orbital modulation, as, for example, polar regions of K star, or shells uniformly surrounding each star, or a shell surrounding the whole system. Therefore, we cannot localize such structures. Our method (and probably any other) cannot distinguish among these solutions without a priori assumptions. Because we start deconvolution assuming a uniform distribution, we preferentially select final solutions with uniformly distributed "halo" emission.

4.2. Modeling of the GIS 2–7 keV Light Curve

The results of the medium-energy X-ray light curve are shown in Figure 3. In contrast to the low-energy solution, the more compact and bright emission regions are now concentrated near to the surface of the K giant. The center of emission denoted by h in Figure 3 corresponds to region b of the SIS solution shown in Figure 2 but is now more compact and shifted toward the K giant. The maxima of these structure are displaced by 0.7 $R_{\odot}$, so that it may not physically be the same region but an adjacent hotter
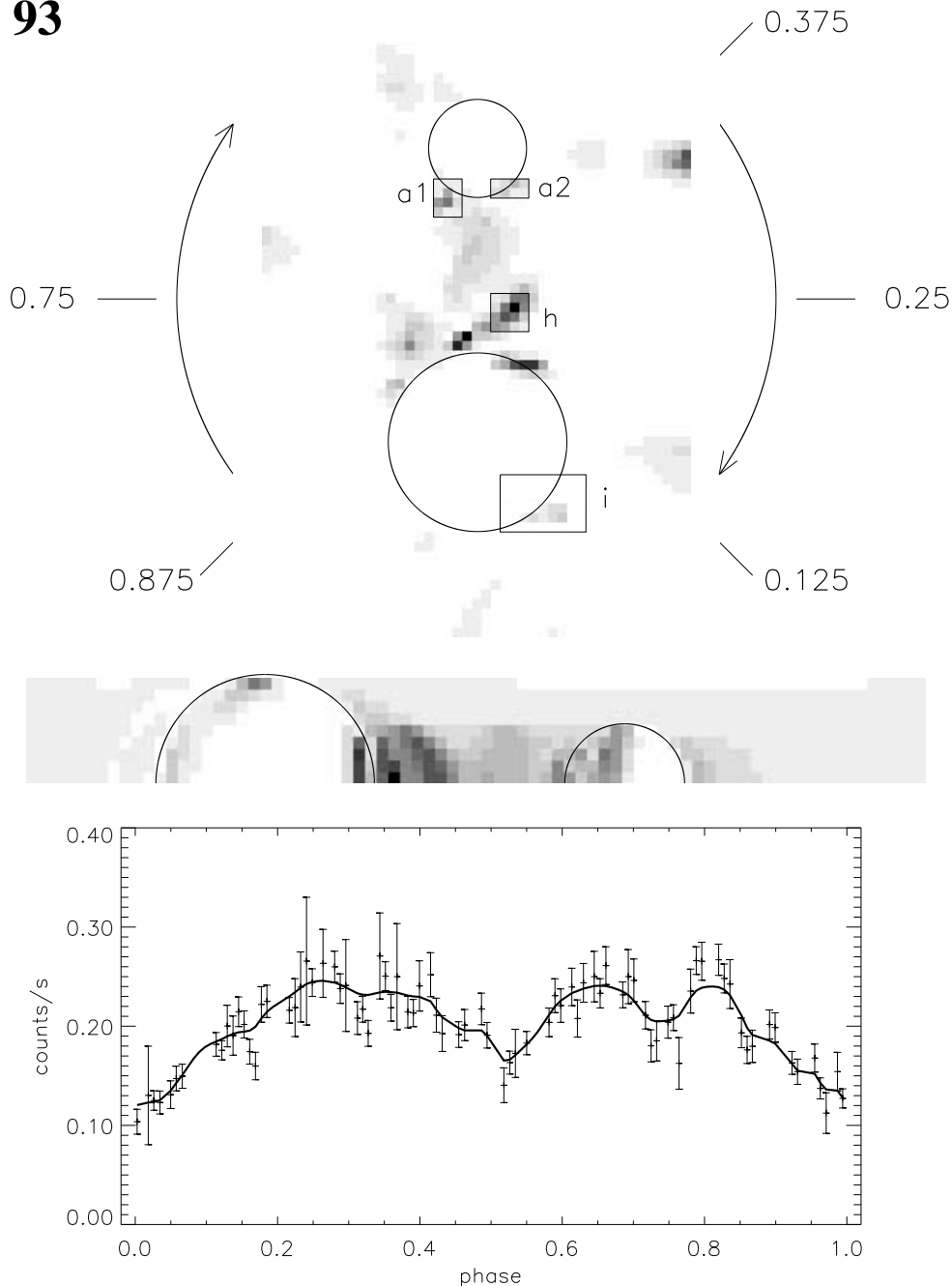

FIG. 3.—Results of the deconvolution of the GIS light curve with most outstanding flares removed, as described in § 2. This solution was obtained in 500 iteration steps. The calculated light curve fits the observed one with a reduced $\chi^2 = 0.97$.

feature. There are four other bright regions located at the K-star surface, three of them (c, d, g) are clearly identifiable in SIS solution. There is no clear concentration of emission in region i in SIS solution. GIS emission connected with G-star is in general weaker. However, the emission of the regions a and f are identifiable in the medium-energy solution. In higher energies lower parts of region a are brighter (we note them as a1 and a2).

The method of deconvolution used is stable against small perturbations of the observed light curve because the largest features are fitted first. This property is useful in making the solutions obtained from the low-energy light curve (which is only slightly disturbed by flares) more stable. On the other hand, the medium-energy light curve may be relatively more contaminated by flares. Any real persistent spatial structure must contribute to the flux at many different phases. This means that the information about localization of any such structure is contained in the whole light curve. This is not true for transient, flarelike features which, if not eliminated from the light curve, can lead to the presence in the images of spurious emission regions. To test for the influence of flares on the medium-energy solution, we have deconvolved the low-energy light curve as presented in Figure 1, without first removing the flares. The result, presented in Figure 4, gives a structure at the same location as bright, highly located region k in the medium-energy solution (Fig. 3). This implies that this structure may be an artifact caused by flares present in the light curve which were not recognized as such and hence were not removed from the light curve used in the analysis. Strong influence of flares can also result in the enhancement of emission at the edges of the volume considered. In the present case, the light curve (Fig. 4) is influenced by flare activity at phases 0.67 and 0.80. These two enhancements lead to artificial depletion in between these phases (phase 0.75), which produces some concentration of emission at the edge of the volume to the right of primary. In the case of the GIS the influence of the same flare is much stronger, and this enhancement is more pronounced. We conclude that these structures in the medium-energy solution, which have counterparts in low-energy solution, are real structures, and the rest of the structures in Fig. 3 are probably artifacts.

Any slow temporal variation in the overall system activity that has a timescale that is similar to the orbital period will produce artifacts in the present (or any other type of deconvolution analysis), as it is modeled as a change due to the eclipse of an emission region. This is why dedicated eclipse mapping/rotational modulation studies of active binary stars (unlike the present *ASCA* observation which was performed in the performance verification phase of the mission) should always cover at least two, and preferably three, orbital periods. Fortunately, the present *ASCA* observation did cover slightly over one orbital period. Comparison of the overlayed parts of light curves indicates that the global levels of activity changed by less than 3% in the SIS light curve and by less than 13% in the GIS light curve between the two orbital periods. These changes are both within the 2 σ error bands (1.3 and 1.7 σ, respectively), and we have implicitly assumed in our modeling that, during this *ASCA* observation, the emission of AR Lac was indeed not affected by any "slow flares" or other types of slow temporal variability.

As previously stated, the 2–7 keV flux is much more sensitive to the hotter plasma component than the 0.4–1.5 keV emission. A comparison of the low- and medium-energy solutions (Figs. 2 and 3) indicates that the emission in the vicinity of the G star is cooler than that near the K star.

4.3. Combined Light Curve Modeling and Inferred Physical Parameters

The global physical parameters of the AR Lac corona have previously been derived using the temperature structure and emission measure distribution inferred from the *ASCA* spectra (Singh et al. 1996; Kaastra et al. 1996). The electron density, N_e, and pressure, P_e, can only be inferred in such studies by making rather arbitrary assumptions about the emitting volume and filling factors. The three-dimensional distribution of emission obtained from our solutions provides a direct estimate of the volume of individual emitting regions and hence the electron density and pressure of the contained plasma. Mapping the emission in two or more well-separated energy bands can provide information on the temperature and emission measure of the emitting plasma in the individual coronal structures based on the ratios of the measured emissions in the maps. The energy bands used here are better separated than most previous observations. However, since even the simplest temperature distribution in the X-ray corona of AR Lac has two temperature components (Singh et al. 1996), and since the low-energy band has significant contributions (§ 2) from both the temperature components, we can only crudely extract the temperature of the plasma based on the hardness ratio alone. Assuming a single-temperature plasma therefore leads to numbers that are only indicative. In these estimations, we used plasma emissivities in the SIS 0.4–1.5 keV and the GIS 2–7 keV energy bands calculated using the chemical abundances presented by Singh et al. (1996). Table 1 summarizes the range of values for the physical parameters obtained for the regions indicated in Figures 2 and 3, for this particular "extended" emission model. The derived temperature range of 1–5 keV is similar to the range of temperatures observed in solar flares, while the values of the electron density obtained are more similar to the range observed in solar active regions (10^9–10^{10} cm^{-3}). In the sixth column the magnetic field strength needed for effective plasma confinement is listed. Some regions are not present in all solutions (e.g., regions b and e are absent in solutions d–f), so the last column in Table 1 lists the range of solutions for which physical parameters were estimated. We also include in Table 1 an estimate of the physical parameters of the halo emission for the emission from the material that is not occulted at the centers of the primary and secondary eclipses. This "halo" is the emission that we cannot localize and can come from plasma that surrounds the system more or less uniformly, or from any other volume that is not occulted by the stars. In these particular estimates of the density and pressure of the "halo" we have assumed that it is spread over the entire volume considered in the modeling.

There is a noticable systematic difference between the temperatures of the low-lying structures associated with the two stars. All of the regions located on the G star have temperatures in the range of 10–30 MK, while most of the regions located at the K secondary have significantly higher temperatures in the range of 20–60 MK. Thus, the corona of the secondary K star appears to be a factor of 2 hotter than that of the primary G star. Since both stars are rotating with the same angular velocity, this difference is presum-
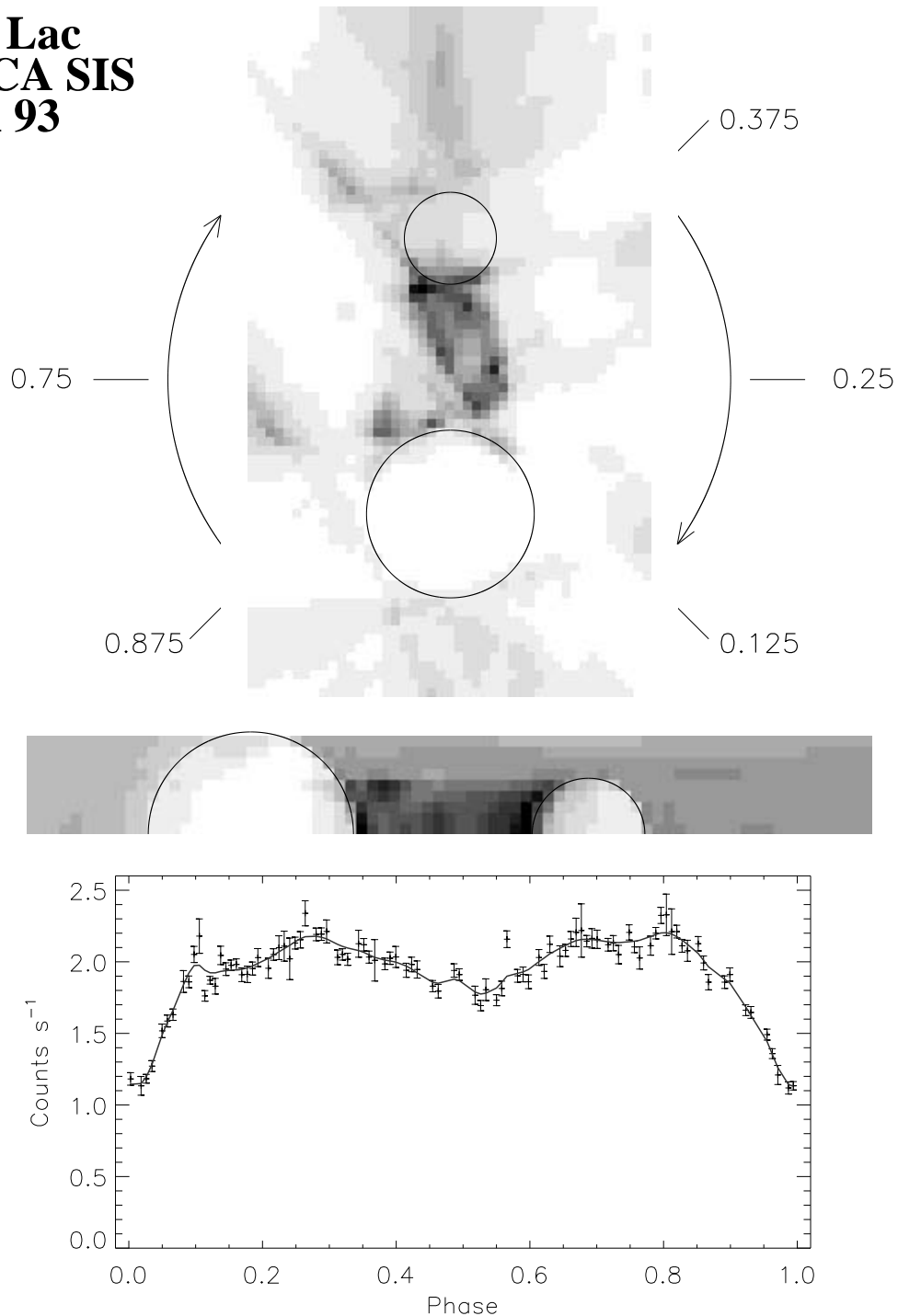
FIG. 4.—Results of the deconvolution of the SIS light curve exactly as it is presented in Fig. 1 (i.e., *without* any of the flares removed). The iteration was stopped at the 800th step when the calculated light curve fitted the observed one with a reduced $\chi^2 = 1.42$.

ably due to some other environmental factor: one possibility is that it is due to the different gravities ($\delta \log g \sim 0.5$) of the two stars.

The lack of eclipses of the high energies observed by the *EXOSAT* ME detector was interpreted by White et al. (1990) and Culhane et al. (1990) as implying that there is a pervasive hot halo component in the RS CVn binaries AR Lac and TY Pyx. In contradiction to this, the present analysis indicates that the halo emission is either the same temperature or somewhat cooler than that of the localized active regions since, in all models where halo emis-

sion is allowed, its temperature is ~ 15 MK. Interestingly, the coolest structure identified in this modeling is the highly elongated region e extending away from the G star on the side opposite to the K star.

4.4. *Spatially Restricted Solutions*

We start the deconvolution process usually from an initially uniform emission distribution. In this approach all possible solutions have the same weights; we do not prefer nor discriminate against the location of any of the emission regions that are required to fit the observed light curve. An

TABLE 1

PARAMETERS OF AR LACERTAE'S CORONAE

Region	T (MK)	EM (10^{52} cm^{-3})	N_e (10^9 cm^{-3})	P (dyne cm^{-2})	B_{conf} (G)	Solutions
a	12–15	18–31	5.4–12	20–46	22–34	a–f
a1	16–28	2.8–11	5.4–13	31–58	28–38	a–f
a2	15–23	1.7–10	5.0–12	26–67	26–41	a–f
a–(a1 + a2)......	7.2–12	7.8–13	4.9–10	13–19	18–22	a–f
b	21–28	6.5–9.2	5.1–6.0	32–47	28–34	a–d
c..................	17–20	5.8–9.0	12–16	62–74	40–43	a–e
d	26–42	4.5–13	4.3–12	49–89	35–47	a–f
e	8.7–9.3	1.8–12	1.2–4.2	2.8–10	8–16	a–c
f	10–12	3.9–55	3.2–18	11–62	17–40	a–f
g	33–64	3.5–17	4.0–11	56–121	38–55	a–f
i	23–54	1.3–14	2.0–11	24–67	25–41	a–f
Halo	14–15	50–78	~9	~6	~12	a–c

alternative approach is to start the iteration process from a nonuniform distribution so as to look for other, less spatially extended solutions. We can assume coronae surround both stars and can thus start the deconvolution from a distribution with intensity that decreases with distance from the stellar surfaces. We can also simply restrict the area of possible solution to some volume around the stars. Figures 5 and 6 present the results of the deconvolution that is
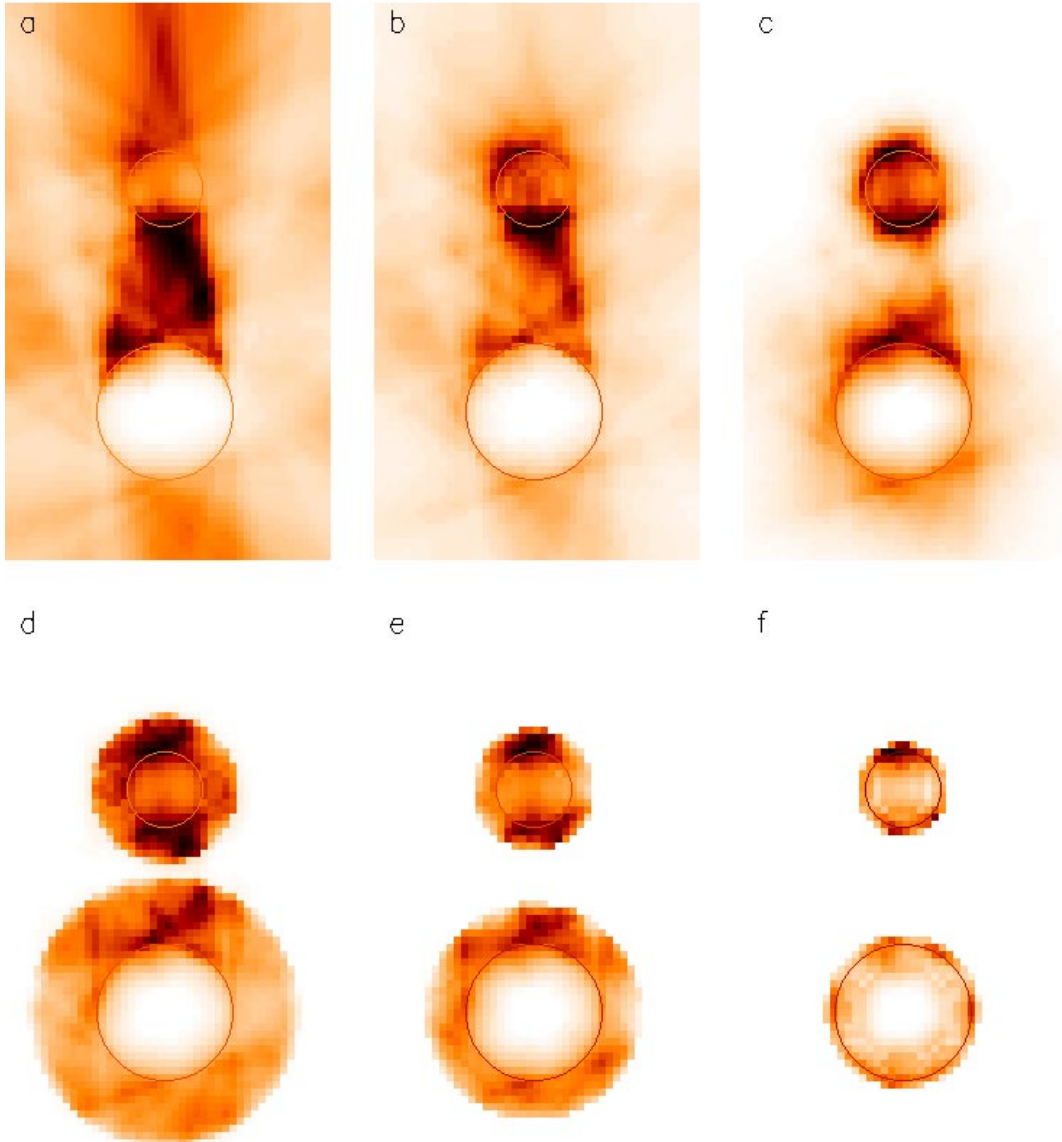

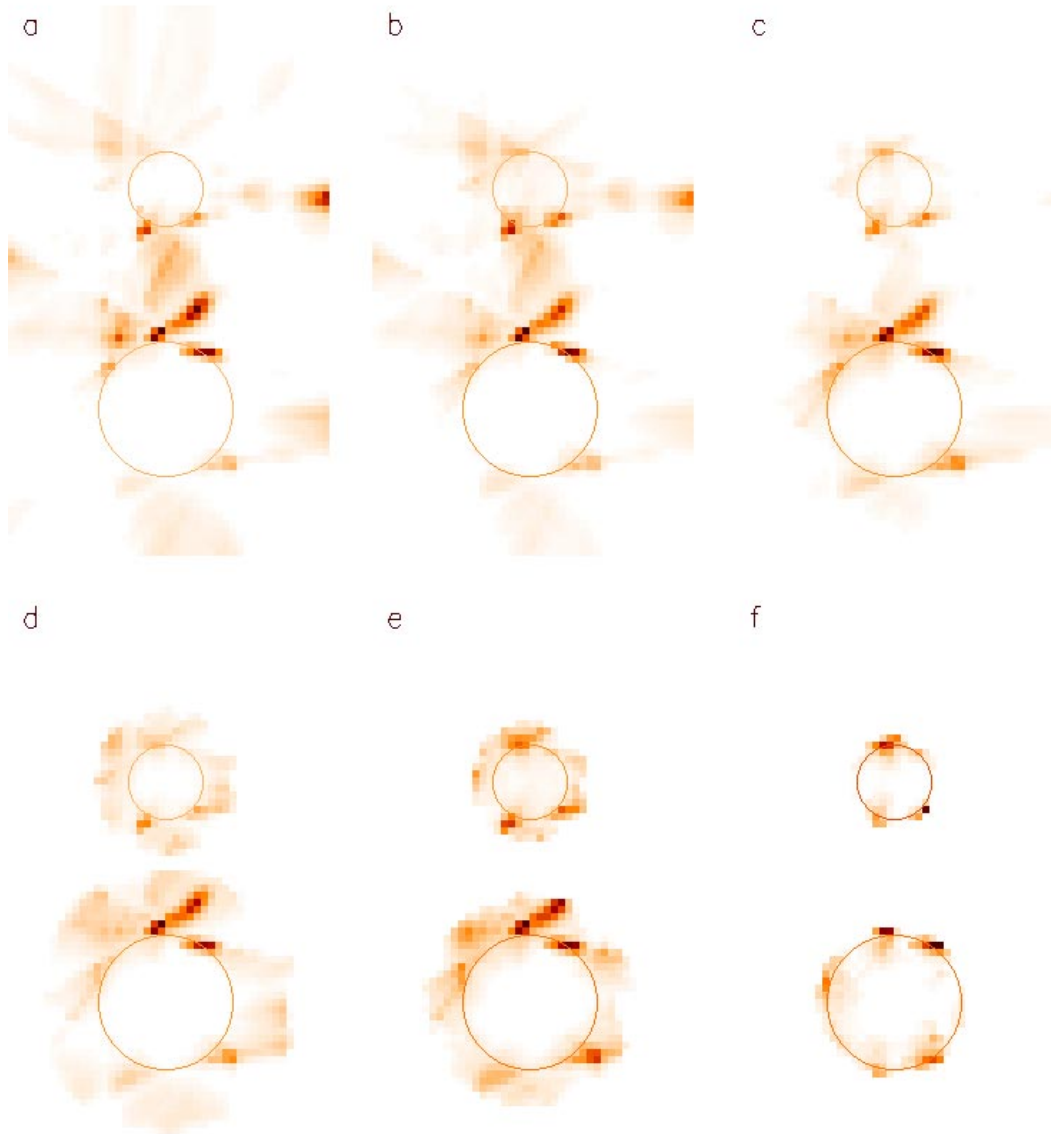FIG. 5.—Comparison of the SIS solutions obtained when starting from differing initial emission distributions

Fɪɢ. 6.—Same as Fig. 5 for the GIS light curve

obtained when one requires that (1) all emitting structures lie within shells of different sizes surrounding both stars (*d, e, f*), or (2) the emission of the initial distributions decays exponentially with height (*b* and *c*). In (*b*) an initial distribution was set according to the predicted pressure scale height of the 7 MK plasma within the system (see § 4); in (*c*), the initial emission distribution was assumed that decays exponentially with height; in (*d*), the initial model was that the two stars were surrounded by uniform shells with heights set equal to the stellar radii; in (*e*), the heights of the shells were set to 0.9 and 1.7 $R_\odot$; finally, in (*f*), the heights of both stellar shells were set to 0.3 $R_\odot$. For comparison, Figures 5*a* and 6*a* show the results of the deconvolutions that were started from uniform spatial distributions.

These examples show that we can indeed obtain acceptable solutions in which only low-lying emission sources are present, with discrete compact structures replacing the extended or linked structures previously found, and with uniform surface coverage replacing the halo emission. Figures 5*d* and 6*d* clearly show that, if we allow the volume considered to extend high enough, high-lying structures are recovered that extend up to the edge of the allowed volume. We can obtain solutions with only low-lying structures, only when we force the extended sources to disappear. It should be noted that in all of the solutions presented in Figures 5 and 6 no "new" regions appeared and that all the regions present, for example, in Figure 6*f*, have counterpart regions that are present in Figures 2 or 3. It is also important that the ratio of GIS and SIS intensities of most of remaining structures is well preserved. The temperatures of most of the regions listed in Table 1 are very similar in all the various solutions, both the previously discussed "extended" models as well as these spatially compact ones.

We have already demonstrated that one can also obtain solutions in which extended emission sources dominate over low-lying, surface structures. In some sense, solutions obtained from uniform initial distributions are the most representative because they contain the whole set of possible emission regions that can explain observed light-curve modulations, but we recognize that there may be other physical reasons, such as electron densities inferred from EUV line ratios (e.g., Dupree et al. 1993), that would argue

in favor of the more compact solutions. We will return to this issue in more detail in the next section.

In all of the above solutions, be they extended or spatially restricted, the coronae are strongly inhomogeneous. We have also searched for solutions having emission that is uniformly distributed on or around the stars and have found that such models cannot explain the observed SIS light curve, giving reduced χ^2 values that are 4.3 or worse. This implies that the best fit for this class of solutions is obtained with coronae extending to $\sim 2.7\,R_\odot$ above the surface of the primary G star and $\sim 0.6\,R_\odot$ above the secondary K star's surface.

5. COMPARISON WITH PREVIOUS ANALYSES OF X-RAY LIGHT CURVES OF AR LACERTAE

In Figure 7 we compare the ASCA 0.4–1.5 keV light curve with the previously obtained EXOSAT LE 0.04–2 keV light curve. It is interesting to note that in the EXOSAT observations, as also in the Einstein and ROSAT observations, the secondary eclipse occurred before phase 0.5, while in the ASCA observation it is a little after the phase 0.5. In addition, the primary minimum in the EXOSAT observation is slightly wider than in the ASCA light curve, and a significant reduction in the X-ray flux during the binary phase 0.66–0.75 seen in the EXOSAT observation is absent in the ASCA light curve. The results obtained here from the ASCA light curve in Figure 7, and those obtained by Siarkowski (1992) from the EXOSAT light curve in Figure 7, are compared in Figure 8 (Plate 15). These two solutions describe the states of the AR Lac corona ~ 9 yr apart. There has been quite a dramatic change in the overall distribution of the X-ray corona. In the ASCA measurement the brightest regions are between the two stars and may be contained in a magnetic structure that links the two stars. In the EXOSAT solution there is also a region of emission that links the two stars, but the two brightest regions are localized on the outer side of the G star and the inward face of the K star.

Ottmann et al. (1993) observed AR Lac in 1990 June using the ROSAT PSPC with low spectral resolution over the energy range of 0.1–2.4 keV. In contrast to the EXOSAT observations, they find that the low- and the high-temperature components are spatially connected and both exhibited eclipses. AR Lac was observed by ROSAT PSPC once more half a year later, in 1990 December during the all-sky survey (cf. Fig. 5 of Schmitt 1992). Analysis of its light-curve modulation performed by Preś et al. (1995a) (see also Siarkowski 1996) indicates the existence of compact emission regions on both stars with localization similar to the positions of active regions indicated by Ottmann et al. (1993). However, contrary to the results of Ottmann et al. (1993), a halo that pervades the system or a similarly unmodulated component of the emission is required. With the limited bandwidth and resolution of ROSAT PSPC it is, however, difficult to separate the low- and high- temperature components using the PSPC (Singh et al. 1996).

Notice that in the EXOSAT, ROSAT, and ASCA solutions, $\sim 50\%$ of the emission is not eclipsed. This is consistent either with an extended halo of emission that pervades the entire system, with emission from the polar regions of the larger K star, or with emission from uniform shells (or from a distribution of many compact coronal structures, as long as it is approximately uniform) around both stars. Whatever the actual configuration, it is interesting that such a large fraction of the X-ray emission is not associated with the discrete, large active regions: even if these latter were somehow to disappear, AR Lac would still be bright in X-rays! The enhancement of the 2–7 keV emission with respect to the lower energy X-ray emission around the K giant suggests that the corona of the K secondary is hotter than corona of the G primary. This possibility was hinted at in the earlier analysis of the Einstein IPC light curve by Walter et al. (1983), who also postulated the existence of extended emission around the K secondary. The lack of any eclipse in the medium-energy EXOSAT ME light curve, and the eclipse mapping by White et al. (1990), likewise suggested a component that is spatially large compared to the overall system dimensions. The change in the 2–7 keV light curve over the 9 yr that separate the EXOSAT and ASCA observations may reflect a change in the temperature distribution of the halo emission.

6. ARE THE CORONAL STRUCTURES IN AR LACERTAE COMPACT OR EXTENDED?

The observed ASCA light curves can be explained by a range of acceptable (at the level of reduced $\chi^2 \approx 1$) solutions. All these solutions are subclasses of our original solution presented in Figures 3 and 4. Both solutions with coronae confined to the stellar surfaces and solutions with large-scale extended coronae are indistinguishable on the basis of the light-curve modulations only. We now present additional arguments based on other considerations that might favor one or other of these alternate classes of solutions.

What evidence and/or arguments are there that favor the coronae of AR Lac being extended? The analysis of the ASCA SIS and GIS spectra of AR Lac by Singh et al. (1996) has shown that the emission can be explained by the presence of two thermal components with temperatures of 7 and 23 MK. For these two temperatures, the corresponding pressure scale heights are 0.9 and 2.9 $R_\odot$ for the G star, and 2.9 and 9.7 $R_\odot$ for the K star, implying that their coronae, if in hydrostatic equilibrium, would be geometrically extended. However, such a simple hydrostatic equilibrium model is known to be unrealistic in that it ignores the controlling influence on the coronal plasma of the strong, local-
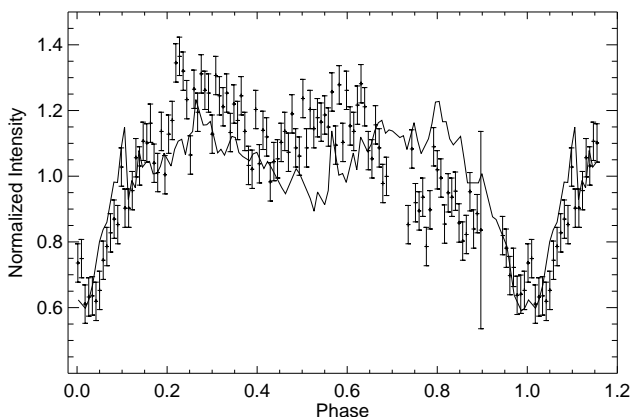

FIG. 7.—Comparison of the low-energy X-ray light curves obtained with the EXOSAT low-energy telescope and the ASCA SIS. The data points with the error bars represent the EXOSAT light curve. The ASCA SIS light curve (Fig. 1 middle panel) is shown as a continuous curve (solid line) without error bars.

ized magnetic fields believed to be present in active stars like AR Lac. In the solar case, we know that the closed magnetic fields of active regions can allow dense, high-temperature plasma to be be retained in low-lying loops whose heights may be much less than the local pressure scale height. There are at least two reasons why we might expect that magnetic loops associated with active regions on RS CVn stars may be much larger than their solar analogs: (1) the spot and plage sizes inferred from photometric modulation and spectral imaging studies of RS CVn stars are 1 order of magnitude or more larger than their solar equivalents, e.g., Neff et al. (1989); assuming a rough proportionality between the horizontal dimensions of an active region and the vertical height H_v of associated coronal loops, this would imply that loop heights $H_v \sim$ 0.1–0.5R_* may be found in RS CVn stars, and (2) in the cases of AR Lac and other RS CVn systems with relatively short orbital periods ($P_{orb} \leq 10$ days), the component stars are close enough together that significant interconnection of magnetic fields associated with active regions on the component stars may occur (cf. Uchida & Sakurai 1984). Such interconnecting field lines should be more or less perpendicular to stellar surfaces, especially on the surfaces of stars that face each other. A rather explicit example of such a structure was inferred by Preś et al. (1995b) for the case of the RS CVn system TY Pyx, based on the shape of the *EXOSAT* X-ray light curve.

There is also observational evidence for the existence of extended coronal structures in AR Lac: the full widths of the primary and secondary eclipses in the *ASCA* light curves are 0.25 and 0.3 orbital phases, respectively, compared to the duration of the optical eclipse of 0.15 (see Fig. 9). The slow egresses and long durations of the X-ray eclipses are most straightforwardly (but not uniquely) interpreted by the coronae around both components being spatially extended: the heights of the coronae corresponding to

these durations are 2.2 and 3.1 $R_\odot$ for the G and K stars, respectively. Bearing in mind that the distance between the stellar surfaces is 4.6 $R_\odot$, this would imply that these coronae most probably merge into each other in a manner similar to that inferred in Figures 2 and 3.

A more indirect argument in favor of an extended corona in AR Lac comes from the estimation of the heights of bright localized chromospheric regions ("plages") made by Neff et al. (1989) using their Mg II spectral imaging analysis. They report that two of the three plages that they inferred to exist on the K star had heights of 0.5R_* above its surface. If there are extended chromospheric regions, it seems highly likely that there will be extended coronal regions. It is also somewhat suggestive that the positions in longitude of these chromospheric plages observed in 1991 December (Neff 1995, private communication) agree well with those of our coronal bright regions c, d, and g (see Figs. 2 and 3) as observed 18 months later.

More general arguments in favor of the existence of extended X-ray emission in RS CVn systems can be made based on the results of very long baseline interferometric (VLBI) radio studies of a number of them, particularly UX Ari. These studies have shown that, at least in some cases, a substantial part of the radio emission originates from structures that are comparable in size to the binary separation (Mutel et al. 1985; Massi et al. 1988; Trigilio, Umana, & Migenes 1993). Drake, Simon, & Linsky (1989, 1992) have demonstrated that there is a strong statistical correlation between the radio and X-ray emissions in a large sample of RS CVn systems, suggesting that the populations of non-thermal radio-emitting electrons and of thermal X-ray emitting electrons are intimately related. Franciosini & Chiuderi Drago (1995) have presented additional arguments in favor of the radio and X-ray emission regions being cospatial in RS CVn systems.

Finally, the timescales for some of the large X-ray flares observed in RS CVn binaries also suggest the existence of large-scale and low-density coronal structures. For example, Kürster (1994) have observed a large X-ray flare with *ROSAT* on the 2.8 day eclipsing RS CVn system CF Tuc that lasted for 9 days. The lack of any obvious eclipses in the X-ray light curves implies that either the flaring region was very extended or that it was located near the polar regions of the stars, according to Kürster. In fact, we would further argue that the protracted timescale of the flare decay by itself is indicative of extended, low-density plasma: if we identify the decay time of this flare as the radiative cooling time of the plasma, this implies plasma densities $\leq 10^9$–10^{10} cm^{-3}. Given that the peak X-ray luminosity of this flare was enormous ($L_X \sim 10^{31.8}$ ergs s^{-1}), implying a large volume emission measure, we estimate that the scale height of the flaring region must have been ≥ 2 $R_\odot$. Other long-duration X-ray "superflares" have been seen in other RS CVn and Algol active binary systems (e.g., a large flare and subsequent enhanced emission lasting over 2 days was observed on AR Lac by Ottmann & Schmitt 1994, a half-day flare of Algol by Stern et al. 1992 and a 3 day flare of HR 5110 by Graffagnino, Wonnacott, & Schaeidt 1995). One can imagine a scenario in which the extended coronae of the stars in an RS CVn system merge to form a circumbinary halo that is perhaps only weakly connected with the system and is intermittently replenished by the material ejected during large flares (White et al. 1990). In the case of AR Lac, for instance, Ottmann &
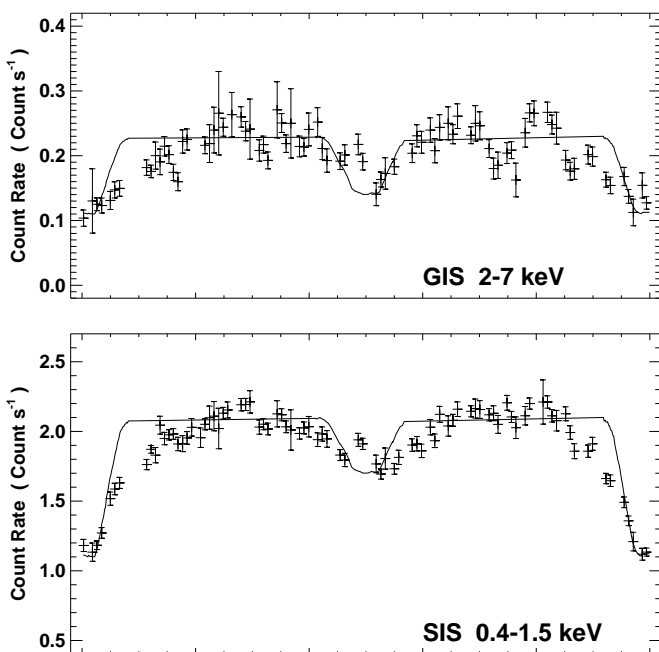
FIG. 9.—Comparison of the optical light curve with the SIS and GIS X-ray light curves. Data points with error bars represent the *ASCA* light curves. The optical light curve (from Kurutaç et al. 1981) is shown as a continuous line.

Schmitt (1994) estimate the frequency at which large flares occur to be about one per two-day orbital period, suggesting that a persistent X-ray halo is quite plausible.

What are the arguments in favor of compact, high-density coronal structures? The existence of short-timescale structures in the X-ray light curves of AR Lac and other RS CVn systems certainly suggests that there can be some relatively compact emission regions but does not necessarily mean that all of the corona is contained in small-scale structures. Indeed, the fact that the X-ray light curve is dominated by long-timescale features would argue that the coronal structures are either extended spatially or, at least, well distributed over the surfaces of the stars. The most compelling arguments for high-density coronal plasma in RS CVn stars are based on $EUVE$ observations of density-sensitive Fe XXI and Fe XXII line ratios: Dupree et al. (1993) infer electron densities $N_e \sim 4 \times 10^{11}$–$1 \times 10^{13}$ at $T_e \sim 10^7$ K in the coronae of the long-period RS CVn Capella, while Schrijver et al. (1995) infer similarly high densities in the corona of the long-period RS CVn system σ Gem. Although these results should be treated with some caution due to the low signal-to-noise ratio of the EUV lines and possible problems of line blending, it does seem that in all active stars which have a significant $\geq 10^7$ K plasma component, the electron densities inferred from these lines are of this order. Given the large coronal emission measure (10^{54} cm^{-3}) of AR Lac, if all of the plasma were in regions with $N_e \geq 10^{12}$ cm^{-3}, the implied scale height $(EM/N_e^2)^{1/3}$ would be $\leq 0.15 R_\odot$, in contradiction to the larger sizes that we have inferred from our light-curve deconvolution.

To summarize, we believe that there is both theoretical and observational support for the existence of geometrically extended structures in the corona of AR Lac. There is also one important class of observation that suggests that the bulk of the high-temperature corona is spatially compact. The resolution of this issue is beyond the scope of this paper, but we would note that reality is usually more complex than the simple models considered here and that there will almost certainly be a range of characteristic sizes for the emission regions in AR Lac's corona, just as there is in the solar corona.

7. CONCLUSIONS

This $ASCA$ observation of AR Lac in two fairly well-separated X-ray bands has provided an opportunity of finding models for the physical parameters of the stellar coronae in this binary system that are consistent with the X-ray light curves. Some conclusions are quite robust while others are quite model-dependent.

The robust results are the following:

1. Both stars are X-ray active, and the corona of the K star secondary component is hotter than that of the G star primary.

2. The X-ray emission tends to be concentrated on the sides of the stars that are facing each other.

3. Comparison with previous AR Lac X-ray observations shows that the pattern of the coronal emission has definitely varied over a timescale of years; there are, however, some features that appear to be present in all of the observations.

4. There are compact, well-localized regions of enhanced X-ray emission with heights well below a stellar radius.

5. About 50% of the emission is not eclipsed, so that its extent or shape is hard to determine. It could be an extended "halo" that pervades the entire system, or be located above the polar regions of the larger K star, or be uniformly covering the surfaces of the two stars. In contradiction to the $EXOSAT$ results, the noneclipsed emission is somewhat cooler than the eclipsed emission regions.

The model-dependent results are the following:

1. In one set of solutions, there is evidence for a region of extended emission linking the two stars, as well as weaker evidence for an elongated emission region above the outward facing side of the G star. The electron densities inferred for these extended structures are similar to the observed range found in (the somewhat cooler) solar active regions, i.e., 10^9–10^{10} cm^{-3}.

2. There is also an acceptable set of models in which only low-lying emission sources are present, i.e., without either extended discrete structures or an extended halo. The electron densities in such models are large ($\geq 10^{12}$ cm^{-3}), but there are some spectral observations of active stars made by $EUVE$ that are consistent with such compact coronal emission regions.

The reality of some of the finer structure evident in the figures is difficult to establish because of the presence of flares and the fact that the observations of AR Lac only extended over one orbital cycle. The next step in the $ASCA$ eclipse-mapping studies would be to obtain X-ray observations over multiple orbital cycles. Such observation would allow us to exclude effects of flares and transient brightenings, and to improve the S/N statistics and the phase coverage, allowing us to somewhat restrict the number of acceptable models. X-ray observations obtained with significantly higher spectral resolution than $ASCA$ by the next generations of X-ray satellites such as $AXAF$ (Canizares 1990) and $NGXO/LAXSM$ (e.g., White et al. 1995) should be able to do significantly better: they will give electron densities directly from density-sensitive line ratios and will also give information on the Doppler shifts of X-ray emitting material, thereby allowing one to (perhaps) uniquely specify which of the acceptable models obtained from eclipse mapping studies of the X-ray light curve is the correct one.

REFERENCES

Canizares, C. R. 1990, Adv. Space Res., 10, 261
Chambliss, C. R. 1976, PASP, 88, 762
Culhane, J. L., White, N. E., Shafer, R. A., & Parmar, A. N. 1990, MNRAS, 243, 424
Drake, S. A., Simon, T., & Linsky, J. L. 1989, ApJS, 71, 905
———. 1992, ApJS, 82, 311
Dupree, A. K., Brickhouse, N. S., Doschek, G. A., Green, J. C., & Raymond, J. C. 1993, ApJ, 418, L41
Franciosini, E., & Chiuderi Drago, F. 1995, A&A, 297, 535
Graffagnino, V. G., Wonnacott, D., & Schaeidt, S. 1995, MNRAS, 275, 129
Kaastra, J. S., Mewe, R., Liedahl, D. A., Singh, K. P., White, N. E., & Drake, S. A. 1996, A&A, in press
Kim, H. 1991, AJ, 102, 1784
Kurutaç, M., Ibanoğlu, C., Tunca, Z., Ertan, A. Y., Evren, S., & Tümer, O. 1981, Ap&SS, 77, 325
Kürster, M. 1994, in Cool Stars, Stellar Systems, and the Sun, ed. J. P. Caillault (San Francisco: ASP), 104
Lemen, J. R., Mewe, R., Schrijver, C. J., & Fludra, A. 1989, ApJ, 341, 474
Massi, M., Felli, M., Pallavicini, R., Tofani, G., Palagi, F., & Catarzi, M. 1988, A&A, 197, 200
Mutel, R. L., Lestrade, J. F., Preston, R. A., & Phillips, R. B. 1985, ApJ, 289, 262
Neff, J. E., Walter, F. M., Rodonò, M., & Linsky, J. L. 1989, A&A, 215, 79
Ottmann, R., & Schmitt, J. H. M. M. 1994, A&A, 283, 871
Ottmann, R., Schmitt, J. H. M. M., & Kürster, M. 1993, ApJ, 413, 710

Popper, D. M. 1980, ARA&A, 18, 115
Preś, P., Siarkowski, M., & Sylwester, M. 1995a, JOSO Annu. Rep. 1994, ed. M. Saniga, 199
———. 1995b, MNRAS, 275, 43
Schmitt, J. H. M. M. 1992, in Rev. Mod. Astron., 5, 188
Schrijver, C. J., Mewe, R., van den Oord, G. H. J., & Kaastra, J. S. 1995, A&A, 302, 438
Siarkowski, M. 1992, MNRAS, 259, 453
———. 1996, in IAU Symp. 176, Stellar Surface Structures, ed. K. G. Strassmeier (Dordrecht: Kluwer), in press
Singh, K. P., White, N. E., & Drake, S. A. 1996, ApJ, 456, 766
Stern, R. A., Uchida, Y., Tsuneta, S., & Nagase, F. 1992, ApJ, 400, 321
Swank, J. H., & White, N. E. 1980, in Cool Stars, Stellar Systems, and the Sun, ed. A. K. Dupree (Cambridge: SAO), 47
Swank, J. H., White, N. E., Holt, S. S., & Becker, R. H. 1981, ApJ, 246, 208
Tanaka, Y., Inoue, H., & Holt, S. S. 1994, PASJ, 46, L37
Trigilio, C., Umana, G., & Migenes, V. 1993, MNRAS, 260, 903
Uchida, Y., & Sakurai, T. 1984, in Activity in Red Dwarf Stars, ed. P. B. Byrne & M. Rodono (Dordrecht: Reidel), 629
Walter, F. M., Gibson, D. M., & Basri, G. S. 1983, ApJ, 267, 665
White, N. E., et al. 1994, PASJ, 46, L97
———. 1995, SPIE, 2518, 59
White, N. E., Culhane, J. L., Parmar, A. N., Kellet, B. J., Kahn, S., van den Oord, G. H. J., & Kuijpers, J. 1986, ApJ, 301, 262
White, N. E., Shafer, R. A., Horne, K., Parmar, A. N., & Culhane, J. L. 1990, ApJ, 350, 776

PLATE 15

EXOSAT LEIT, 4 July 84
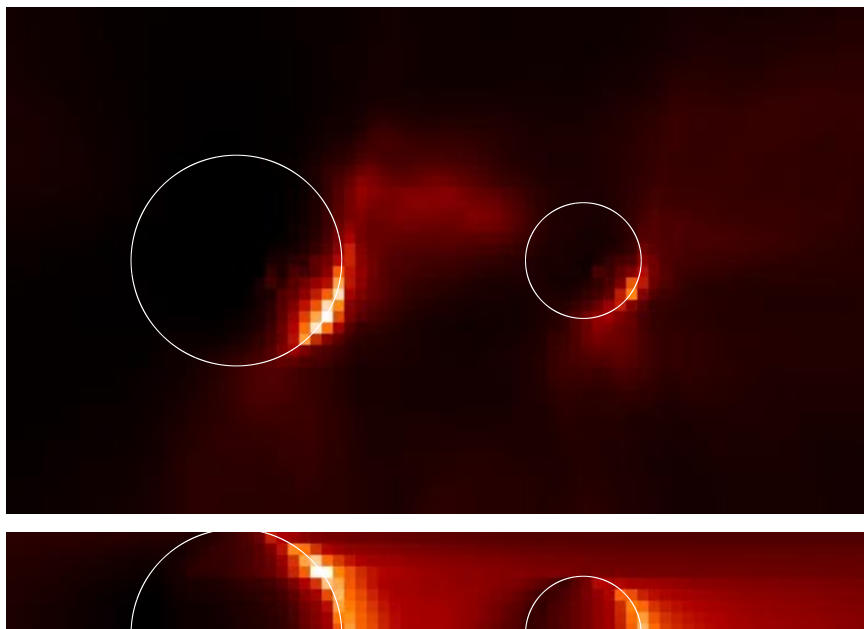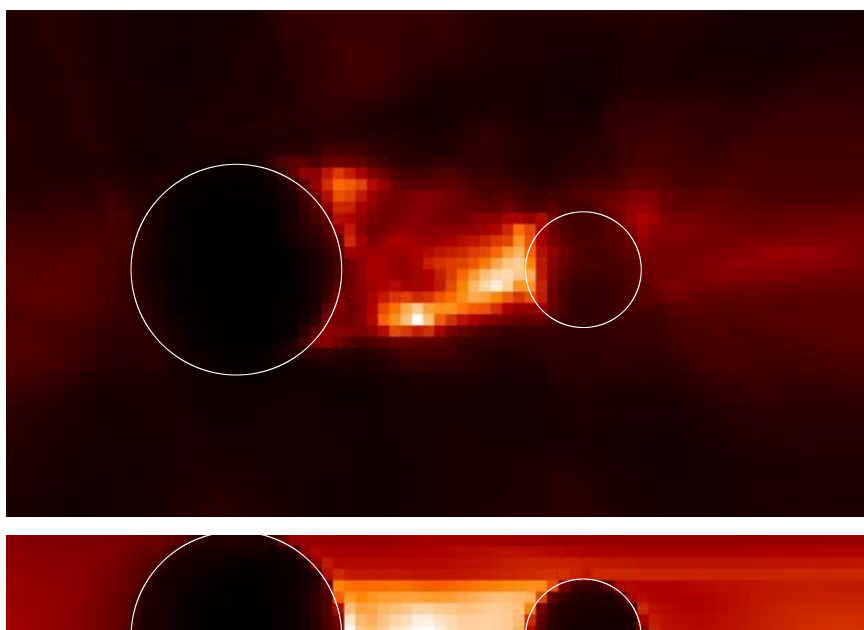

ASCA SIS, 4 June 93

Fig. 8.—Comparison of the structure of AR Lac's corona at two epochs separated by an interval of 9 yr. The left panel shows the solution obtained from the *EXOSAT* LE (0.04–2 keV) light curve (Siarkowski 1992), while the right panel shows the SIS (0.4–1.5 keV) solution from this paper. For both of the panels, a top view and a side view for phase 0.25 (90°) are shown.

Siarkowski et al. (see 473, 479)